Molecular Therapy
Oncolytics
Original Article

AMERICAN SOCIETY of GENE & CELL THERAPY

# Oncolytic Herpes Simplex Virus Inhibits Pediatric Brain Tumor Migration and Invasion

Julia V. Cockle,[1,2] Anke Brüning-Richardson,[1] Karen J. Scott,[1] Jill Thompson,[3] Timothy Kottke,[3] Ewan Morrison,[4] Azam Ismail,[5] Angel M. Carcaboso,[6] Ailsa Rose,[1] Peter Selby,[1] Joe Conner,[7] Susan Picton,[2] Susan Short,[1] Richard Vile,[1,3] Alan Melcher,[1,8,9] and Elizabeth Ilett[1,9]

[1]Leeds Institute of Cancer and Pathology, University of Leeds, Leeds LS9 7TF, UK; [2]Yorkshire Regional Centre for Paediatric Oncology and Haematology, Leeds General Infirmary, Leeds LS1 3EX, UK; [3]Department of Immunology, Mayo Clinic, Rochester, MN 55905, USA; [4]Leeds Institute of Biomedical and Clinical Sciences, University of Leeds, Leeds LS9 7TF, UK; [5]Department of Pathology, St. James's University Hospital, Leeds LS9 7TF, UK; [6]Institut de Recerca Sant Joan de Deu, Barcelona 08950, Spain; [7]Virttu Biologics, Glasgow G11 6NT, UK; [8]Institute of Cancer Research, London SM2 5NG, UK

**Pediatric high-grade glioma (pHGG) and diffuse intrinsic pontine glioma (DIPG) are invasive tumors with poor survival. Oncolytic virotherapy, initially devised as a direct cytotoxic treatment, is now also known to act via immune-mediated mechanisms. Here we investigate a previously unreported mechanism of action: the inhibition of migration and invasion in pediatric brain tumors. We evaluated the effect of oncolytic herpes simplex virus 1716 (HSV1716) on the migration and invasion of pHGG and DIPG both in vitro using 2D (scratch assay, live cell imaging) and 3D (spheroid invasion in collagen) assays and in vivo using an orthotopic xenograft model of DIPG invasion. HSV1716 inhibited migration and invasion in pHGG and DIPG cell lines. pHGG cells demonstrated reduced velocity and changed morphology in the presence of virus. HSV1716 altered pHGG cytoskeletal dynamics by stabilizing microtubules, inhibiting glycogen synthase kinase-3, and preventing localized clustering of adenomatous polyposis coli (APC) to the leading edge of cells. HSV1716 treatment also reduced tumor infiltration in a mouse orthotopic xenograft DIPG model. Our results demonstrate that HSV1716 targets the migration and invasion of pHGG and DIPG and indicates the potential of an oncolytic virus (OV) to be used as a novel anti-invasive treatment strategy for pediatric brain tumors.**

## INTRODUCTION

Pediatric high-grade glioma (pHGG) and diffuse intrinsic pontine glioma (DIPG) are invasive tumors associated with poor survival.[1,2] Despite intensive treatment with surgery, radiotherapy, and chemotherapy, 5-year survival for pHGG remains low, at 15%–35%.[1,3] DIPG is a major cause of neuro-oncology-related death in childhood, with over 90% of children dying within 2 years of diagnosis.[4–6] Standard treatment for DIPG includes 6 weeks of radiotherapy to stabilize disease, prevent early progression, and improve neurological function; however, the effect on overall survival is minimal.[4] There is clearly a pressing clinical need to develop novel therapeutic strategies to improve outcomes for these patients and one such avenue is to target pHGG and DIPG migration and invasion,[7] a well-known characteristic of glioma cells.[8,9]

Oncolytic virotherapy offers a novel treatment approach for pHGG and DIPG. Oncolytic viruses (OVs) are anti-cancer agents that are capable of selectively infecting and lysing cancer cells, while leaving normal tissue unharmed.[10,11] Alongside their ability to kill infected cancer cells, OVs can also generate an anti-cancer immune response, by enhancing the immunogenicity of the tumor microenvironment and activating innate and adaptive immune responses against infected tumor cells.[11] Thus, OVs have huge clinical potential for poor prognosis tumors through their ability to act as selective cytotoxic and immunogenic agents.

However, very little is known about the effects of OVs on cancer cell invasion and migration. Given that the cytoskeleton plays a critical role in regulating the life cycle of infecting viruses,[12–15] OVs may be able to influence cancer cell migration through their interplay with the host cancer cell cytoskeleton. If OVs have the potential to inhibit cancer cell migration and invasion, this might contribute to their therapeutic potential for poor prognosis invasive tumors such as pHGG and DIPG.

In this study, we demonstrate that oncolytic herpes simplex virus 1716 (HSV1716) can specifically inhibit pHGG and DIPG migration and invasion, highlighting a novel mechanism of action for an OV against a principal hallmark of cancer. HSV1716 was evaluated in this study, as it has previously been applied in early-phase trials for high-grade gliomas.[16–20] We also demonstrate that HSV1716 can alter pHGG cytoskeletal dynamics, stabilizing microtubules and altering molecular pathways critical for cell polarity, migration, and movement. Finally, we show that infection of tumor cells with HSV1716 reduced tumor infiltration in a mouse orthotopic xenograft model of DIPG.

Received 16 April 2017; accepted 25 April 2017;
http://dx.doi.org/10.1016/j.omto.2017.04.002.

[9]These authors contributed equally to this work.

**Correspondence:** Julia V. Cockle, Leeds Institute of Cancer and Pathology, University of Leeds, Leeds LS9 7TF, UK.
**E-mail:** juliacockle@doctors.net.uk

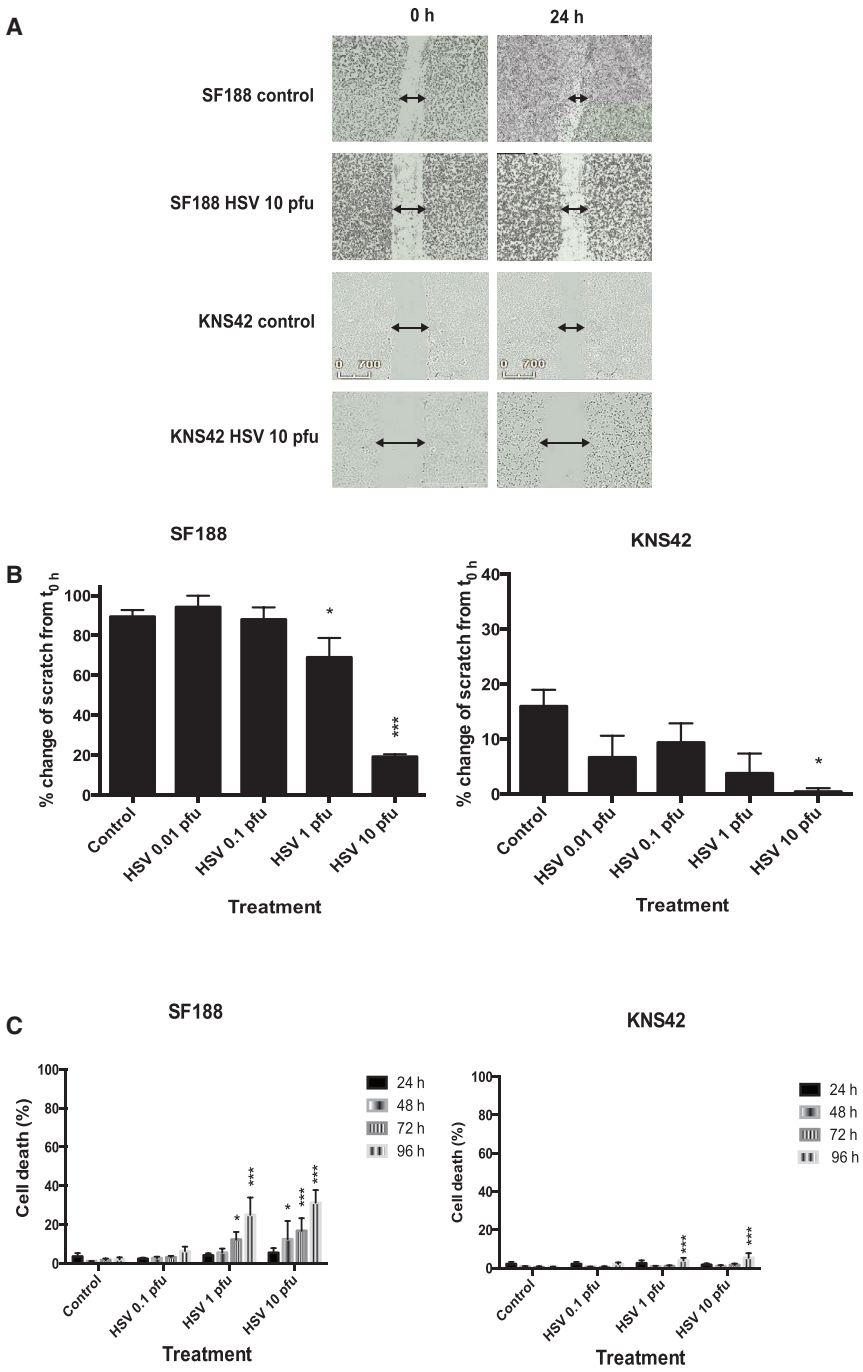


**Figure 1. Oncolytic HSV1716 Can Inhibit Migration of pHGG Cell Lines**

Cell lines (SF188 and KNS42) were seeded into 24-well plates at 1 × $10^5$ cells/well. After 24 hr, a scratch was applied across the monolayer and wells were treated with or without HSV1716 at 10 PFU/cell. (A) Plates were imaged at ×4 magnification in the IncuCyte ZOOM incubator. Images shown are representative stills from movies of SF188 and KNS42 created with IncuCyte software at time 0 hr and 24 hr post-treatment. (B) Plates were imaged at 0 hr and 24 hr using the EVOS cell imaging system at ×4 magnification. Migration was quantified from images using ImageJ software to determine the percent change in the area of the scratch over 24 hr. Graphs show means ± SEM from three individual experiments (*$p < 0.05$ and ***$p < 0.001$ by one-way ANOVA). (C) Cells (SF188, KNS42) were seeded at 1 × $10^5$ cells/well in a 12-well plate, left to adhere, and then incubated with or without HSV1716 at 0.1, 1, 10, or 50 PFU/cell. At 24, 48, 72, or 96 hr, cells were harvested, washed, and stained with LIVE/DEAD cell stain. The percentage of dead cells was determined by FACS analysis. Graphs show means ± SEM of three individual experiments (*$p < 0.05$ and ***$p < 0.001$ by two-way ANOVA).

## RESULTS

### Oncolytic HSV1716 Can Inhibit Migration of pHGG Cell Lines in a 2D Scratch Assay

The ability of HSV1716 to block the migration of two pHGG cell lines (SF188 and KNS42) was evaluated using a scratch assay (Figure 1A). HSV1716 at 1 or 10 plaque-forming units (PFU)/cell significantly reduced the migration of SF188 cells, and HSV1716 at 10 PFU/cell significantly reduced migration of KNS42 cells at 24 hr post-infection (Figure 1B).

To verify that the anti-migratory effect was not a direct consequence of cytotoxicity, cell viability was investigated using a LIVE/DEAD assay (Figure 1C). At 24 hr (the time point for analysis of the scratch assay), cell viability was not significantly affected by HSV1716, with fewer than 6% dead cells being detected (Figure 1C). Additionally, pHGG cell proliferation, as determined by the Ki67 intracellular fluorescence-activated cell sorting (FACS) assay, was not significantly affected at 24 hr by HSV1716 treatment (data not shown).

Although significant cytotoxic effects were observed in SF188 cells at later time points following treatment with HSV1716 (Figure 1C), the level was quite low, with less than 40% cell death seen at 96 hr post-infection. KNS42 cells were highly resistant to HSV1716-induced cytotoxicity, with very low levels of cell death observed at 96 hr after infection. Nonetheless, this indicates a potential dual mechanism of action for HSV1716 via inhibition of tumor cell migration and also via direct cytotoxic effects.

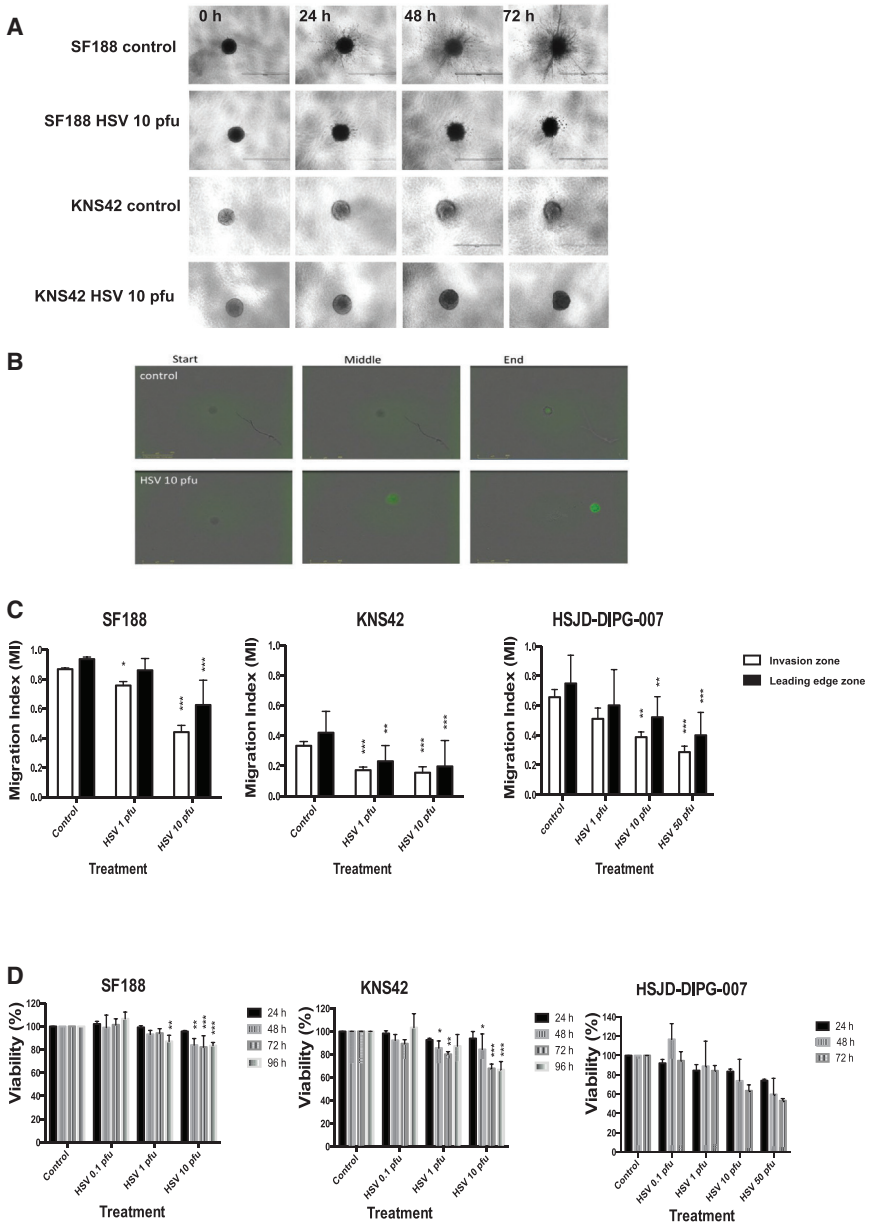


**Figure 2. Oncolytic HSV1716 Can Inhibit Invasion of pHGG and DIPG Tumor Spheroids**

Tumor spheroids (SF188, KNS42, DIPG) were encased in collagen and incubated with or without HSV1716 at 10 PFU/cell for 72 hr. (A) SF188 and KNS42 tumor spheroid invasion was evaluated at 24, 48, and 72 hr using the EVOS cell imaging system at ×4 magnification. The white scale bar represents 1,000 μm. Images shown are representative of three individual experiments. (B) SF188 tumor spheroids were encased in collagen and incubated with or without HSV1716-GFP at 10 PFU/cell. Plates were imaged at ×4 magnification using the IncuCyte ZOOM incubator over 70 hr. Images shown are representative stills from movies created with IncuCyte software, which were taken at around 0, 36, and 70 hr post-treatment. The yellow scale bar represents 800 μm. (C) Images generated from the EVOS cell imaging system at 72 hr as described in (A) were analyzed using ImageJ software by calculating the area of the invasion zone and the leading edge zone. A MI for both the invasion zone and the leading edge zone ((area of zone – area of core) ÷ total area) was calculated. Graphs show means ± SEM of multiple repeats pooled from up to three individual experiments (*$p < 0.05$, **$p < 0.01$, ***$p < 0.001$ by one-way ANOVA). (D) Cells (SF188, KNS42, DIPG) at $1 \times 10^3$ cells/well were seeded in an ultra-low attachment round-bottom 96-well plate to form spheroid aggregates. Following 72-hr incubation, cells were incubated with or without HSV1716 at 0.1, 1, and 10 PFU/cell. Cell viability at 24, 48, 72, and 96 hr post-infection was determined by WST-1 assay and is expressed as a percentage of controls. Graphs show means ± SEM of three individual experiments for SF188 and KNS42 and two experiments for DIPG (*$p < 0.05$, **$p < 0.01$, ***$p < 0.001$ by two-way ANOVA).

### Oncolytic HSV1716 Can Inhibit Invasion of pHGG and DIPG Cell Lines in 3D Spheroid Assays

A 3D tumor spheroid assay was used to investigate the effects of oncolytic HSV1716 on pHGG and DIPG invasion. Tumor spheroids of each cell line (SF188, KNS42) were encased in a collagen matrix and then overlaid with HSV1716 at varying concentrations. Tumor spheroid invasion was imaged over 72 hr using the EVOS cell imaging system (Figure 2A). A migration index (MI) was calculated from the images obtained and was used to evaluate the invasion front and leading edge zone for each treatment. As previously described, these zones are defined as the area into which the bulk of migrating cells (75%) move and the area containing all the migrating cells, respectively. To evaluate whether HSV1716 could penetrate the collagen matrix and infect cells, tumor spheroids were encased in collagen and overlaid with medium containing HSV1716-GFP at 10 PFU/cell. GFP expression within SF188 spheroids was detected within 36 hr (Figure 2B).

HSV1716 significantly reduced invasion of pHGG and DIPG tumor spheroids by 72 hr (Figure 2C). A statistically significant reduction in both the invasion zone and leading edge zone at 72 hr was observed following treatment with HSV at 10 PFU/cell for SF188 (means ± SEM are given unless otherwise indicated; leading edge: control, 0.94 ± 0.004; and HSV at 10 PFU/cell, 0.63 ± 0.047; $p < 0.001$) and DIPG (leading edge: control, 0.75 ± 0.051; HSV at 10 PFU/cell, 0.52 ± 0.038; $p = 0.0061$; and HSV at 50 PFU/cell, 0.40 ± 0.041; $p < 0.001$). KNS42 spheroids appeared to be more sensitive to HSV1716 and infection at 1 PFU/cell resulted in significant inhibition of migration (KNS42 leading edge: control, 0.42 ± 0.033; HSV at 1 PFU/cell, 0.23 ± 0.029; $p = 0.0014$; and HSV at 10 PFU/cell, 0.20 ± 0.05; $p < 0.001$). The observed effects were not

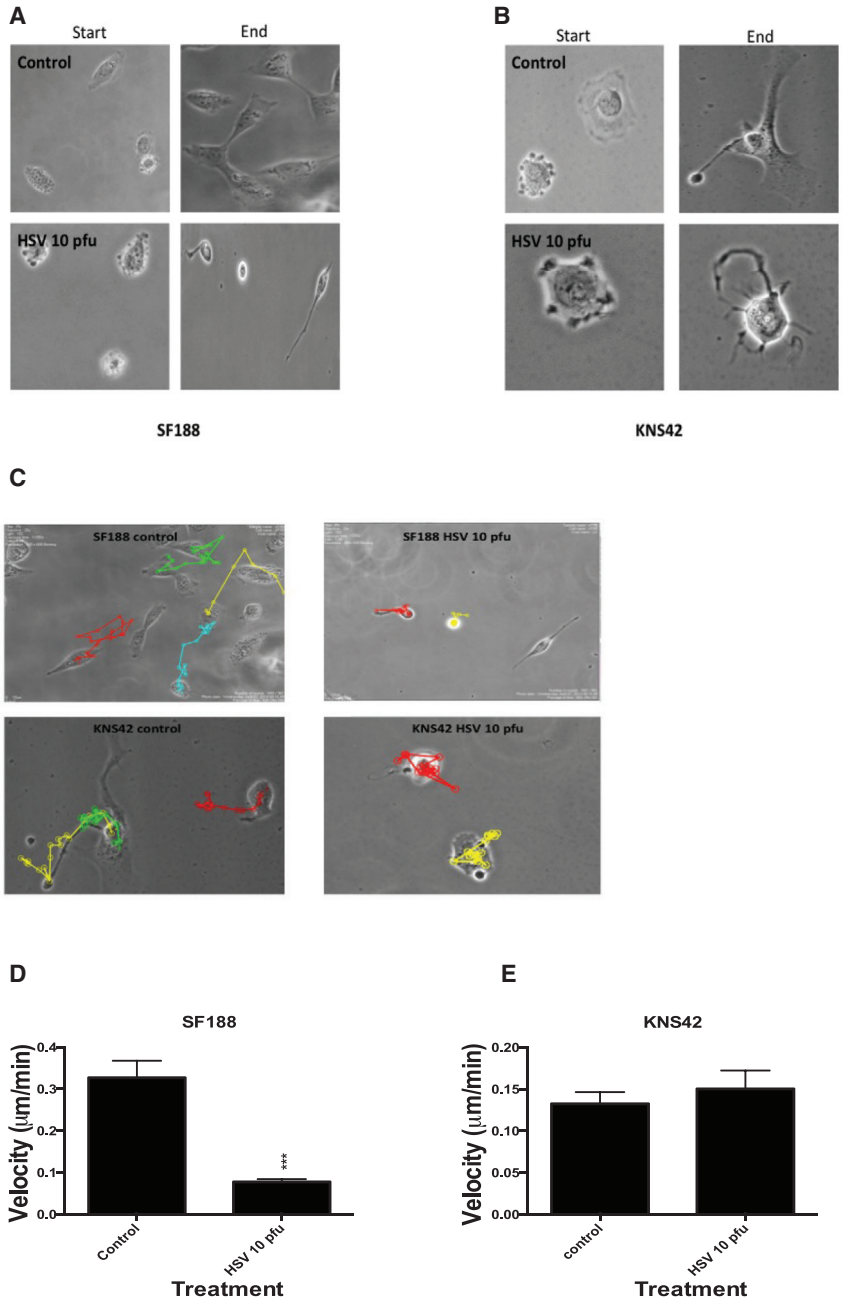


**Figure 3. Live Cell Imaging of pHGG Cell Lines Reveals Differences in Cell Morphology and Velocity Following Oncolytic HSV1716 Treatment**

(A and B) Pediatric glioma cell lines SF188 (A) and KNS42 (B) were incubated with or without HSV1716 at 10 PFU/cell in an Ibidi imaging dish. Live cell imaging was performed for 48 hr using the Nikon Biostation IM live cell imaging system. Magnification ×40. Stills were taken from time 0 hr at 2-hr intervals from movies of SF188 (A) and starting at 12 hr post-imaging start for KNS42 to allow for the reduced motility of this cell line in comparison to SF188. (C) Tracking analysis of the individual cell movements over 48 hr of SF188 and KNS42 was performed from live cell imaging movies using ImageJ with MTrack software following treatment with or without HSV1716. (D and E) Quantification analysis of velocity was obtained from live cell imaging using ImageJ with MTrack software of both cell lines following treatment with or without HSV1716. Graphs show the means ± SEM obtained from five different fields of view (***$p < 0.001$ by Student's two-tailed t test).

due to the cytotoxic activity of the virus because the changes in migration were generally greater than the loss of viability (Figures 2C and 2D). For SF188 cells, there was an 8.13% or a 33.30% reduction in the leading edge zone versus the control and a 10.13% or 41.30% reduction in the invasion zone versus control, compared to 10.79% or 15.36% loss of viability for 1 PFU/cell and 10 PFU/cell, respectively, at 72 hr. For KNS42 cells, there was a 44.97% or 53.11% reduction in the leading edge zone versus the control and a 48.50% or 53.30% reduction in the invasion zone versus the control, compared to a 19.86% or 32.12% loss of viability for 1 PFU/cell and 10 PFU/cell, respectively, at 72 hr. For DIPG cells, there were 19.68%, 30.43%, and 46.57% reductions in the leading edge zone versus the control and 22.23%, 41.00%, and 56.35% reductions in the invasion zone versus control compared to a 15.78%, 36.56%, and 46.87% loss of viability for 1, 10, and 50 PFU/cell, respectively, at 72 hr. Proliferation, as determined by spheroid core size change over time, did not increase significantly following HSV1716 treatment (data not shown).

### Oncolytic HSV1716 Can Alter pHGG Cell Morphology, Velocity, and Polarity

Given the data above showing that HSV1716 reduced the migration and invasion of glioma cells, we hypothesized that we should see direct changes in cell morphology, velocity, and polarity following virus treatment.

To address this question, SF188 and KNS42 were incubated with or without HSV1716 at 10 PFU/cell and time-lapse imaging was performed over 48 hr (Movies S1, S2, S3, and S4). Virus treatment markedly changed pHGG cell morphology (Figures 3A and 3B). Untreated SF188 cells were highly motile and polarized, with a distinct front-rear axis defining a leading protrusive front and a trailing edge. The cell leading edge clearly protruded as filopodia and lamellipodia and the trailing edge tail visibly retracted, progressing the cell forward. After treatment, SF188 cells were notably less motile and demonstrated a pronounced loss of polarity and a change in morphology. SF188 HSV-treated cells became elongated with a loss of their distinct leading and trailing edge and developed protrusive tails that were unable to retract. Following HSV treatment, the

SF188 cells appeared anchored to the surface and were unable to generate the coordinated contractile forces required to propel the cell forward. As previously documented, KNS42 cells were observed to be overall much less motile than SF188. Untreated KNS42 cells appeared to have diffuse, extended, and well-defined lamellipodia, which, unlike SF188, appeared to be orientated in opposite directions with no clear front-rear definition. HSV1716 treatment of KNS42 cells resulted in cells rounding up with no discernable lamellipodia, and the cells instead developed multiple thin-branching protrusions (Figure 3B).

Tracking analysis confirmed that pHGG cells treated with HSV1716 were much less motile than corresponding controls (Figure 3C). A statistically significant reduction in cell velocity was observed in HSV1716-treated SF188 cells, although not in KNS42 cells (Figures 3D and 3E) (SF188 mean velocity: control, 0.33 ± 0.041 μm/min; and HSV, 0.078 ± 0.007 μm/min; $p < 0.001$; KNS42 mean velocity: control, 0.13 ± 0.014 μm/min; and HSV, 0.15 ± 0.022 μm/min; $p = 0.506$).

### Oncolytic HSV1716 Stabilizes pHGG Microtubules through Accumulation of Post-translational Tubulin Modifications

Microtubules are polymers of α- and β-tubulin dimers that bind to form stiff cylindrical hollow tubes that play a critical role in cell migration.[21] Microtubules are dynamic and can undergo polymerization (growth) and depolymerization (shrinkage) during a process known as dynamic instability, in order to search, explore, and interact with cellular organelles and target sites.[21–24] While the majority of microtubules undergo dynamic instability with a relatively short half-life, a subgroup of more "stable" microtubules demonstrate longer half-lives. This increased microtubule stability is directly reflected through the accumulation of post-translational tubulin modifications including acetylation and detyrosination.[21,24,25] These more stable microtubules are more resistant to disassembly and can facilitate directional trafficking and preferential transportation of organelles, vesicles, or proteins within the cell.[21,24,26,27] However, accumulation of such post-translational modifications has been shown to reduce focal adhesion turnover and subsequent cell migration.[28] It is postulated that more "dynamic" microtubules are required for cell migration.[29–31] Therefore, the ability of HSV1716 to stabilize pHGG microtubules through the accumulation of post-translational tubulin modifications was evaluated by western blotting and immunofluorescence (IF). The expression of acetylated tubulin from pHGG cell lysates treated with HSV at 10 PFU/cell was evaluated by western blot, which showed that virus treatment of SF188 and KNS42 cells somewhat increased the levels of acetylated tubulin at 24 and 48 hr (Figure 4A).

Acetylated and detyrosinated tubulin levels from pHGG cells treated with or without oncolytic HSV1716 at 10 PFU/cell were quantified by IF after 24 and 48 hr. Taxol was used as an internal control, as it is a known microtubule stabilizing agent.[32] HSV1716 treatment of SF188 cells at 10 PFU/cell resulted in a statistically significant increase in both acetylated and detyrosinated tubulin levels at 24 and 48 hr compared to controls (mean intensity normalized to control: acetylated tubulin at 24 hr: control, 1 ± 0.785; and HSV, 513 ± 135, $p = 0.00427$; acetylated tubulin at 48 hr: control, 1 ± 0.523; and HSV, 246 ± 60.8; $p < 0.001$; detyrosinated tubulin at 24 hr: control, 1 ± 0.983; and HSV, 62.4 ± 22.2; $p = 0.0186$; detyrosinated tubulin at 48 hr: control, 1 ± 0.397; and HSV, 4.5 ± 0.594, $p < 0.001$) (Figures 4B–4E). The effects of HSV treatment on SF188 acetylated and detyrosinated tubulin levels were more marked than the effects of 100 nM Taxol.

HSV1716 treatment of KNS42 cells significantly increased acetylated tubulin at 48 hr (mean intensity normalized to control for acetylated tubulin at 24 hr: control, 1 ± 0.997; and HSV, 11.5 ± 5.02; $p = 0.0672$; acetylated tubulin at 48 hr: control, 1 ± 0.804; and HSV, 6,038 ± 2,272; $p = 0.0289$) (Figure 4D). KNS42 appeared to be more sensitive to the effects of Taxol than SF188, with statistically significant increases in both acetylated and detyrosinated tubulin following 24 and 48 hr of treatment (mean intensity normalized to control: acetylated tubulin at 24 hr: control, 1 ± 0.997; and Taxol, 24.8 ± 5.8; $p = 0.00258$; acetylated tubulin at 48 hr: control, 1 ± 0.804; and Taxol, 5,727 ± 709; $p = < 0.001$; detyrosinated tubulin at 24 hr: control, 1 ± 0.099; and Taxol, 1.35 ± 0.12; $p = 0.04$; detyrosinated tubulin at 48 hr: control, 1 ± 0.084; and Taxol, 1.81 ± 0.34; $p = 0.0475$) (Figures 4D and 4E). HSV1716 did not significantly increase KNS42 expression of detyrosinated tubulin (Figure 4E). This is also in keeping with a drug screen published by canSAR (http://cansar.icr.ac.uk) that identifies Taxol as a potent inhibitor of KNS42.

### Oncolytic HSV1716 Can Decrease pHGG Glycogen Synthase Kinase-3β Activity and Prevent Adenomatous Polyposis Coli Localization

Glycogen synthase kinase (GSK)-3 is a serine/threonine protein kinase that plays a key role in orchestrating cell migration through regulation of cell structure, motility, adhesion, and cytoskeleton dynamics.[33–35] We previously demonstrated the importance of GSK-3 in pHGG cell migration and invasion.[7] In a study designed to investigate the mechanism of wild-type HSV spread, HSV was shown to induce the formation of stable microtubule subsets through inactivation of GSK-3β in normal human dermal fibroblasts.[14] Since the effects of HSV1716 on GSK-3 expression in human tumor cells are currently unknown, we examined them in our pHGG cell lines.

HSV1716 treatment of SF188 or KNS42 cells appeared to increase levels of the inactivated form of GSK-3β (phosphorylated GSK-3β Ser9) and this effect was more marked at 24 hr than at 48 hr (Figure 5A). By contrast, HSV1716 treatment resulted in a trend toward decreased levels of the activated form of GSK-3αβ (Tyr216/279 phosphorylated GSK-3αβ) for both pHGG cell lines at 24 and 48 hr (Figure 5B). Overall, HSV1716 treatment resulted in a trend toward decreased total GSK-3β levels over 48 hr for both pHGG cell lines (Figure 5C). Although the majority of the results described above did not reach statistical significance, they do represent a consistent trend that fits with the biological hypothesis, and small differences in kinase activity may have large biological consequences. In addition,

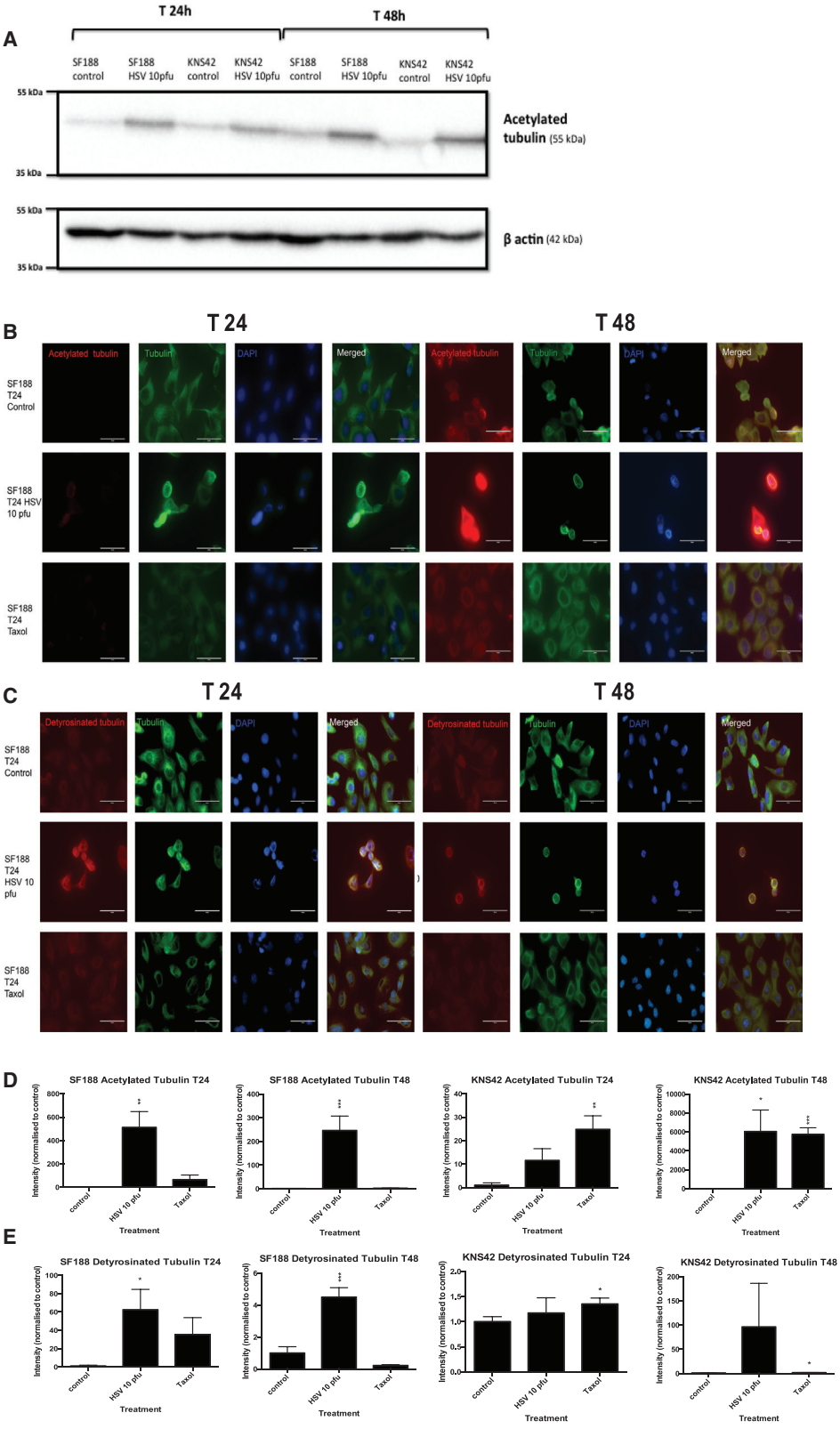


*(legend on next page)*

the techniques employed here measure total levels of cellular GSK-3β activity, whereas morphologically localized modulation of the activity of this kinase was previously shown to be functionally significant in migrating cells;[21,33] this phenomenon could well be happening in the cells examined here. This is accumulating support that oncolytic HSV can decrease GSK-3β activity in pHGG cells, increasing the inactive GSK-3 isoform and reducing the activating tyrosine of GSK-3αβ.

GSK-3 plays an important role in regulating the polarity of migrating cells.[33,36] Polarity cues result in the localized inhibition of GSK-3, which promotes adenomatous polyposis coli (APC) clustering at microtubule plus ends at the leading edge of cells, controlling the direction of movement.[36] Given that HSV1716 appears to decrease GSK-3β activity in pHGG cells, we hypothesized that HSV1716 treatment of pHGG cells would alter APC intracellular distribution.

Untreated SF188 cells demonstrated a clear localization of APC to the leading edge of cells (Figure 5D). This effect was not notable for KNS42, possibly a reflection of the fact that this cell line was much less motile than SF188 (Figure 5D). Following treatment with HSV1716, SF188 cells demonstrated diffuse staining of APC throughout the cytoplasm, with a clear loss of APC clustering to a leading edge (Figure 5D). A similar diffuse distribution of APC was seen in SF188 cells treated with the GSK-3 inhibitor 6-bromoindirubin-oxime (BIO).

### Oncolytic HSV1716 Treatment Reduced Tumor Infiltration and Enhanced Therapy in a Mouse Orthotopic Xenograft Model of DIPG

An orthotopic xenograft model of DIPG was established by injecting HSJD-DIPG-007 cells into the fourth ventricle of non-obese diabetic severe combined immunodeficiency (NOD SCID) mice, allowing tumor cell growth and invasion into the brainstem. To evaluate the effects of HSV1716 in this model, either HSJD-DIPG-007 cells premixed with PBS (control) or HSJD-DIPG-007 cells premixed with HSV1716 at 10 PFU/cell were injected.

Analysis of mouse brain sections from the control group showed a moderate increase in cellularity within the brainstem, adjacent cortex, and cerebellum by diffusely infiltrating sheets of atypical glial cells (Figures 6A and 6B). These cells had hyperchromatic and moderately pleomorphic nuclei and fine fibrillary cytoplasm (Figure 6C). Mitotic activity was high with no evidence of necrosis or vascular proliferation. These HSJD-DIPG-007 tumor cells did not form a solid mass but appeared to migrate, invade, and infiltrate diffusely throughout the midbrain, medulla, and cerebellum following their injection into the brainstem (Figures 6A and 6B). Cell invasion reached the subpial surface, where the cells then continued to spread horizontally in clusters (Figure 6D).

Conversely, the brain sections obtained from mice that received an intracranial injection of HSJD-DIPG-007 premixed with HSV1716 demonstrated well-contained collections of increased cellularity within the brainstem, with very limited infiltration into the surrounding structures (Figure 6E). These well-contained collections consisted of abnormal-looking cells with elongated nuclei and mixed with apoptotic bodies, indicative of tumor cells (Figures 6F and 6G).

## DISCUSSION

pHGG and DIPG are highly aggressive tumors associated with diffuse infiltrative growth patterns.[8,9] This invasive phenotype contributes toward limited therapeutic response and, as such, there is a clear need to develop new clinical therapies that effectively target tumor migration and invasion. Oncolytic virotherapy for pHGG is under-researched compared to adult brain tumors and there are currently no published studies reporting the effects of OVs on DIPG. Furthermore, there are no reported studies evaluating the effects of OVs on pHGG or DIPG migration and invasion, making our study highly novel. We have shown that the OV HSV1716 can inhibit the in vitro migration and invasion of pHGG and DIPG cells. This is of high translational relevance, as any residual cells resistant to the cytotoxic effects of concomitant chemotherapy or OV would be unable to subsequently infiltrate normal surrounding brain tissue, allowing for the possibility of more targeted radiotherapy or second-look surgery, potentially improving outcomes.

The possible mechanism by which HSV1716 may reduce pHGG migration and invasion was also explored. HSV1716 altered pHGG cytoskeletal dynamics, stabilizing microtubules through the accumulation of post-translational tubulin modifications. Furthermore, HSV1716 altered molecular pathways critical for cell polarity, migration, and movement. Virus treatment of pHGG cell lines resulted in a tendency toward inhibited GSK-3β activity and prevented the localized clustering of APC to the leading edge of the cell, a process dependent on localized modulation of GSK-3β function.[36]

It is known that dynamic microtubules are required for cell migration.[29–31] The accumulation of post-translational modifications such as acetylated tubulin, which marks microtubules as stable, have been shown to reduce focal adhesion turnover and subsequent cell migration.[28] Viruses have the ability to hijack components of

**Figure 4. Oncolytic HSV1716 Stabilizes pHGG Microtubules through Accumulation of Post-Translational Tubulin Modifications**

(A) pHGG cell lines SF188 and KNS42 were treated with or without HSV1716 at 10 PFU/cell. Following either 24- or 48-hr incubation, cell lysates were prepared and expression of acetylated tubulin was determined by western blotting. (B and C) $2 \times 10^5$ cells (SF188 and KNS42) were grown on sterile coverslips and treated with or without HSV1716 at 10 PFU/cell or 100 nM Taxol for 24 or 48 hr. The effects of treatment at 24 and 48 hr on acetylated tubulin (B) and detyrosinated tubulin (C) expression were evaluated by IF labeling, shown here for SF188. Red labeling, acetylated or detyrosinated tubulin; green labeling, tubulin; and blue labeling, DAPI staining. Magnification ×63. White scale bars represent 50 μm. (D and E) Between 40 and 80 cells from each treatment condition were evaluated to determine the intensity of acetylated (D) and detyrosinated (E) tubulin labeling normalized to the control at 24 and 48 hr. Error bars show means ± SEM (*$p < 0.05$, **$p < 0.01$, ***$p < 0.001$ by Student's two-tailed t test).

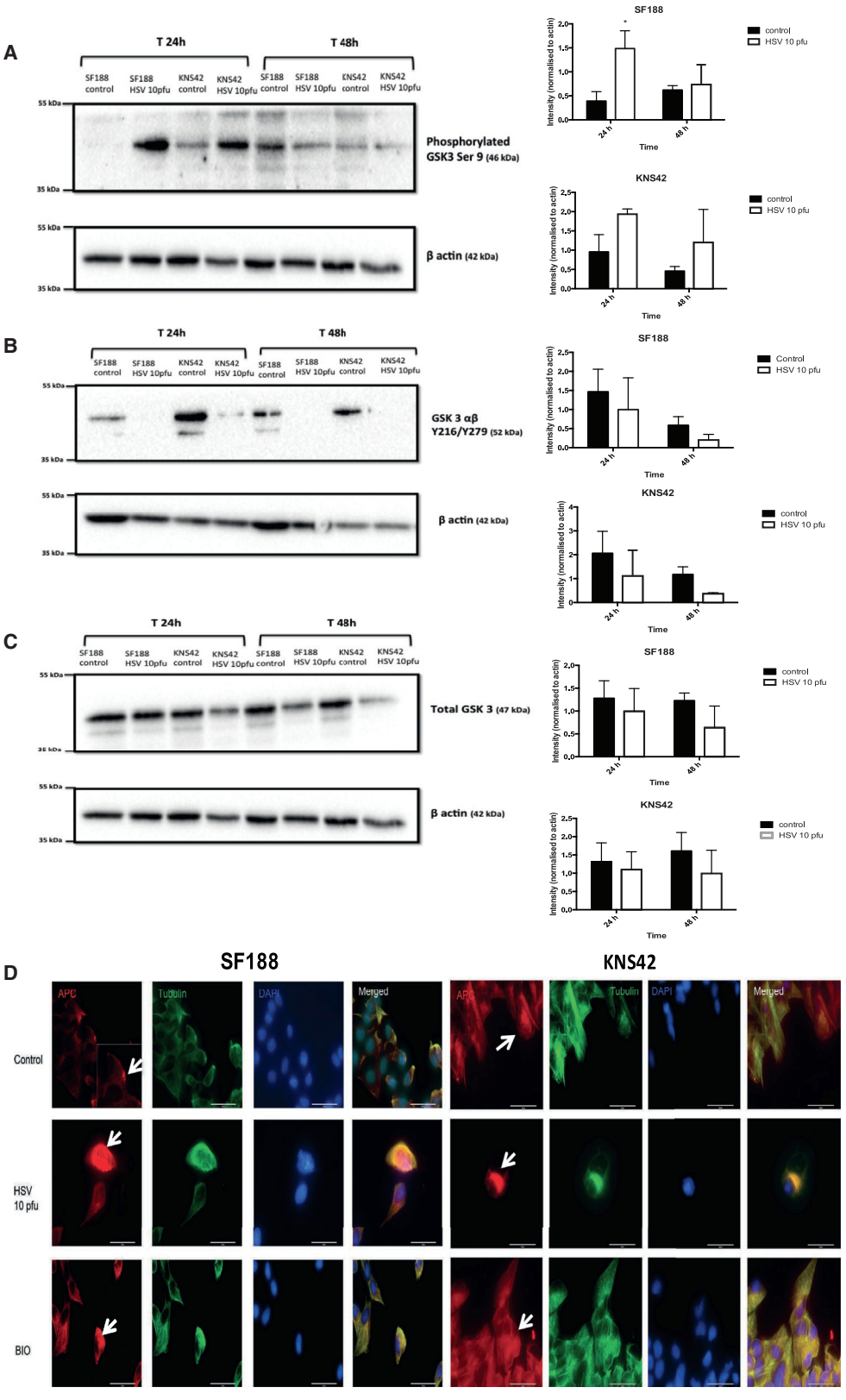


*(legend on next page)*

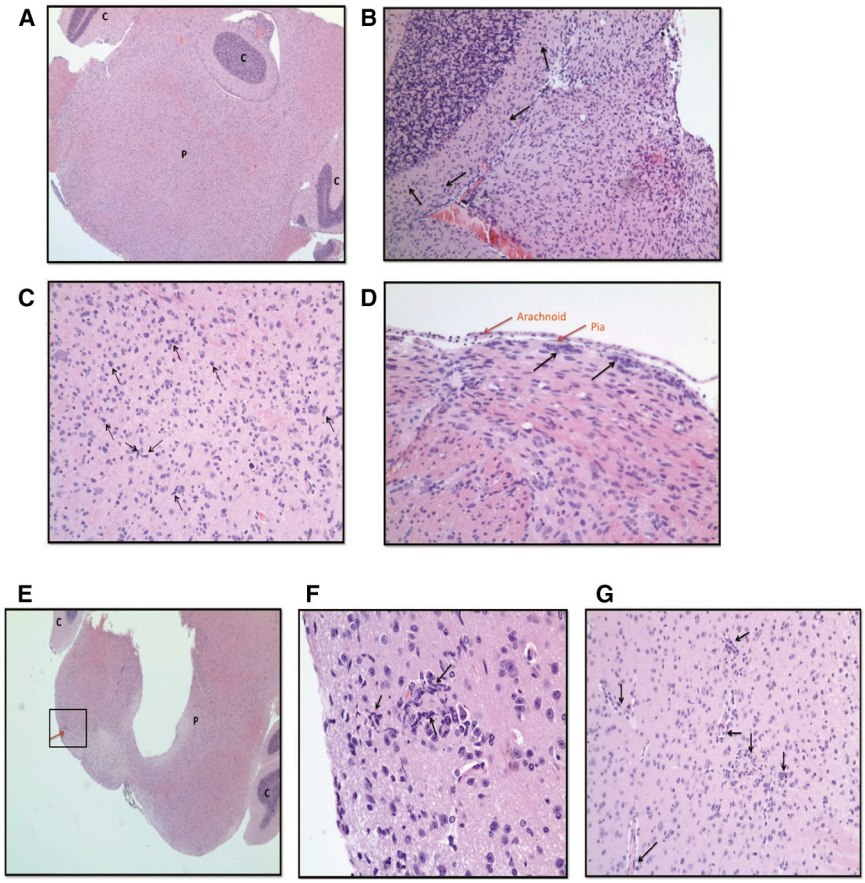


**Figure 6. Oncolytic HSV1716 Reduced Tumor Infiltration in a Mouse Orthotopic Xenograft Model of DIPG**

(A–G) 5 × $10^5$ disaggregated DIPG cells premixed with PBS (A–D) or HSV1716 at 10 PFU/cell in PBS (E–G) were stereotactically injected into the brains of 4- to 5-week-old NOD SCID mice. Tumors were allowed to establish and mice were euthanized when they showed signs of disease (i.e., severe ataxia or > 15% weight loss). Brains were harvested into 4% PFA, sliced into coronal sections, embedded in paraffin, and sectioned to 4-μm thickness. Tissue sections were stained with H&E. Images were taken using the SPOT Insight camera and Leitz DMRB microscope. Images from mouse brain obtained on day 62 post-surgery (A–D), day 123 post-surgery (E and F), and day 78 post-surgery (G). (A) Brainstem section at ×2.5 magnification. (B) Section through the cerebellum at ×10 magnification. (C) Brainstem section of pons at ×20 magnification. (D) Section showing arachnoid and pia at ×20 magnification. Black arrows show representative examples of diffusely infiltrating atypical glial cells. (E) Cross-section of pons and cerebellum at ×2.5 magnification. Red arrow indicates a well-contained section of abnormal-looking cells. (F) ×40 magnification of the boxed area in (E). (G) Brainstem section at ×20 magnification. Black arrows show representative examples of diffusely infiltrating atypical glial cells. C, cerebellum; P, pons.

the cytoskeleton in order to facilitate their replication cycle and spread, and this phenomenon has been reported for wild-type HSV.[14] Oncolytic HSV1716 also appears capable of stabilizing microtubules, through accumulation of post-translational modifications such as acetylated and detyrosinated tubulin in pHGG cells, and this process may explain the reduction in pHGG motility, migration, and invasion observed.

We previously showed that GSK-3β plays a key role in pHGG cell migration and invasion.[7] Our data suggest that HSV1716 may facilitate microtubule stabilization, and hence inhibit pHGG migration and invasion, by increasing levels of the inactive form of GSK-3β. These results are in keeping with the work of Naghavi et al.,[14] who showed that wild-type HSV-1 infection of primary human cell lines can result in inactivation of GSK-3β by the action of the viral serine/threonine kinase Us3, leading to the formation of stable microtubules. Future work is required in order to further explore this mechanism using our virus in a pediatric brain tumor model. In addition, we observed that the localized clustering of APC to the leading edge of the cells was disrupted, a process that is dependent on functional GSK-3β.[36] The diffuse cellular APC localization may explain the observed loss of cell polarity.

Finally, the ability of oncolytic HSV to inhibit glioma invasion was explored in vivo. Mice receiving intracranial injection of DIPG cells premixed with HSV1716 showed evidence of reduced tumor infiltration in an orthotopic xenograft model of DIPG compared to controls. This work forms part of ongoing efforts to develop in vivo models of

**Figure 5. Oncolytic HSV1716 Can Decrease pHGG GSK-3β Activity and Prevent APC Localization**

pHGG cell lines SF188 and KNS42 were treated with or without HSV1716 at 10 PFU/cell. (A–C) Following either 24- or 48-hr incubation, cell lysates were prepared and expression of phosphorylated GSK-3β Ser9 (inactivated form) (A), Tyr216/279 phosphorylated GSK3αβ (active form) (B), and total GSK-3β (C) was determined by western blotting. The β-actin control was included to evaluate protein loading and transfer. Intensity of each band was quantified and normalized to the β-actin control using ImageJ software. Graphs show means ± SEM of three individual experiments (*$p < 0.05$ by Student's two-tailed t test). (D) 2 × $10^5$ cells (SF188 or KNS42) were grown on sterile coverslips and treated with or without oncolytic HSV at 10 PFU/cell or 5 μM BIO for 24 hr. The effects of treatment at 24 hr on APC localization (white arrows) were evaluated by IF labeling. Red labeling, APC; green labeling, tubulin; and blue labeling, DAPI staining. Magnification × 63. White scale bars represent 50 μm.

glioma invasion in order to efficiently screen novel anti-invasive therapies for pediatric brain tumors.

Oncolytic virotherapy offers a completely novel treatment approach for poor prognosis children's brain tumors. Although clinical experience for use in children with intracranial tumors is limited to a few case reports,[37] promising results have been demonstrated in adult patients with high-grade glioma in terms of safety, tolerability, and multiple dose delivery.[16–20] Virus delivery across the blood-brain barrier and to specific areas of the brain, including the brainstem in the case of DIPG, must also be considered; however, novel techniques such as positive pressure infusion using convection-enhanced delivery may be able to enhance viral distribution and target delivery.[38] Additionally, for pHGG, intra-operative delivery of HSV1716 to the residual macroscopic tumor or the tumor cavity would be a possibility, overcoming the need for virus to cross the blood-brain barrier.

We show here, for the first time to our knowledge, that HSV1716 may also have a role as an anti-invasive therapeutic. As such, oncolytic HSV may have the potential to reduce tumor migration and infiltration from post-operative residual cancer cells. This additional mechanism of action against a principle hallmark of cancer further highlights the huge clinical potential for such oncolytic virotherapy. Furthermore, this anti-invasive mechanism of action could be valuable in the treatment of highly invasive tumors such as DIPG, which are not amenable to surgical options.

Our data therefore support the case for the development of the clinical application of oncolytic virotherapy for pHGG and DIPG and highlight the therapeutic potential of an OV not only as a cytotoxic and immunogenic treatment but also as an anti-invasive strategy.

## MATERIALS AND METHODS

### Cell Lines

Cell lines used in this study were the pediatric glioma cell lines SF188 and KNS42 (a kind gift from Prof. Chris Jones, Institute of Cancer Research) and the patient autopsy-derived DIPG cell line HSJD-DIPG-007 (a kind gift from Dr. Angel M. Carcaboso) hereafter referred to as DIPG. Cell line identity (SF188 and KNS42) was verified by serial tandem-repeat profiling (in-house testing at the Cancer Research UK Leeds Centre genomics facilities). SF188, KNS42, and DIPG cell lines were cultured as previously described.[7] All cell lines were tested and shown to be free of mycoplasma contamination.

### Virus

Oncolytic HSV1716 (which carries the *ICP34.5* deletion of a neurovirulence gene to enhance safety) at a stock concentration of $1 \times 10^9$ PFU/mL was obtained from Virttu Biologics and stored at −80°C in PBS. A GFP-expressing HSV1716 (HSV1716-GFP) was also obtained from Virttu Biologics at the same stock concentration.

### Scratch Migration Assay

Cells were seeded at $1 \times 10^5$ cells/well into 24-well plates (Corning) such that after 24 hr of growth, they reached 80%–90% confluence as a monolayer. After 24-hr incubation at 37°C, a line was drawn on the underside of each well across the center with a fine marker. A scratch was applied across the center of the monolayer, perpendicular to the marker line. After detached cells were removed, culture medium with or without HSV1716 at 50, 10, 1, 0.1, and 0.01 PFU/cell was added. Migration of cells across the scratch was determined by imaging at 0 hr and 24 hr with the EVOS cell imaging system (Thermo Fisher Scientific) at ×4 magnification. Migration was quantified using ImageJ software (https://imagej.nih.gov/ij; NIH) to determine the percent change in the area of the scratch from time zero to 24 hr.

### Spheroid Invasion Assay

Spheroids were generated as previously described.[7] Spheroids embedded in collagen were incubated in 100 μL cell culture medium with or without HSV1716 at $8 \times 10^2$, $8 \times 10^3$, $8 \times 10^4$, or $4 \times 10^5$ PFU/well, which approximates to a nominal 0.1, 1, 10, or 50 PFU/cell. Spheroid expansion and invasion into the collagen matrix was imaged and analyzed as previously described[7] and the MI for 3D migration was determined. Two zones of migration were defined: the invasion zone, representing the area outside the spheroid core into which approximately 75% of migrating cells invaded; and the leading edge zone, representing the total area containing migrated cells. The MI was calculated as ((area of zone − area of spheroid core) ÷ total area).

### Live Cell Imaging of Adherent Cells

10 μL cells in 500 μL culture medium was placed in two of four quadrants of an Ibidi imaging dish (Nikon) and allowed to adhere for 2 hr at 37°C. Equal volumes of medium were replaced in one quadrant with HSV1716 at an approximation of 10 PFU/cell. The Ibidi dish was then cultured in the incubation/imaging chamber of the Nikon Biostation IM live cell imaging system. Cells were imaged for 48 hr at 3-min intervals at 37°C with 5% $CO_2$ in air. Cell tracking and analysis was carried out according to Cockle et al.[7] For tracking, the nucleus of each cell was identified and tracked over the 48-hr period at 150-min intervals using ImageJ with MTrack software (Biomedical Imaging Group Rotterdam).

### Live Cell Imaging of Spheroids

HSV1716 infection of spheroids was assessed by GFP expression within spheroids infected with HSV1716-GFP. Collagen was overlaid with cell culture medium with or without $8 \times 10^4$ PFU/well of HSV1716-GFP. Spheroids were imaged in the IncuCyte ZOOM incubator (Essen BioScience) at 37°C with 5% $CO_2$ in air using the ×4 microscope objective, with images taken hourly for 70 hr. IncuCyte software (Essen BioScience) was used to create movies and visualize GFP expression.

### WST-1 Assay

$1 \times 10^3$ cells/well in culture medium were seeded in an ultra-low attachment round-bottom 96-well plate to form spheroid aggregates. Following 72-hr incubation at 37°C, cells were treated with an equal volume of culture medium with or without $8 \times 10^2$, $8 \times 10^3$, $8 \times 10^4$,

or $4 \times 10^5$ PFU/well of HSV1716. At 24-hr intervals for up to 96 hr, 10 μL water soluble tetrazolium-1 (WST-1) (Roche) was added per well and, after 4 hr, absorbance at 450 nm was detected using the colorimetric microplate reader. Spheroid imaging and analysis was according to Cockle et al.[7]

### LIVE/DEAD Assay

Cells were seeded into 12-well plates (Corning) at $1 \times 10^5$ cells/well in 2 mL culture medium and left to adhere for a minimum of 4 hr at 37°C. Culture medium with or without HSV1716 at 50, 10, 1, 0.1, and 0.01 PFU/cell was then added to each well. Cells were harvested, washed in PBS, and stained with LIVE/DEAD red fixable stain according to the manufacturer's instructions (Thermo Fisher Scientific). Cells were washed, fixed in 1% paraformaldehyde (PFA) (Sigma-Aldrich), and stored at 4°C until acquisition on the Attune flow cytometer (Thermo Fisher Scientific). Analysis was carried out using Attune Flow Cytometric software (version 2.1; Thermo Fisher Scientific).

### Immunofluorescence

To investigate the effects of HSV1716 on tubulin acetylation and detyrosination, cells were treated with or without either HSV1716 at 10 PFU/cell or 100 nM Taxol (Selleckchem) for 24 to 48 hr. To evaluate the cellular location of APC, cells were grown under the same conditions and treated with or without either HSV at 10 PFU/cell or 5 μM BIO for 24 hr (Calbiochem).

Antibodies for IF studies were rat anti-tubulin fed following treatment with (1:500; Serotec), mouse anti-acetylated tubulin (1:500; Sigma-Aldrich), rabbit anti-detyrosinated α-tubulin (1:200; Abcam), rabbit polyclonal M-APC (1:2,000; a kind gift from Prof. Inke Näthke), and secondary antibodies at 1:500 (Alexa Fluor-conjugated reagents; Molecular Probes). Nuclear staining was performed with DAPI (Molecular Probes) at the recommended working concentrations.

For IF studies of acetylated and detyrosinated tubulin, the fluorescence intensity of each image was calculated in ImageJ software using a standard threshold across all images. The fluorescence intensity was then divided by the number of cells in each image to calculate the intensity of acetylated or detyrosinated tubulin per cell.

### Western Blotting

Cells were treated with or without HSV1716 at 10 PFU/cell and harvested at 24 or 48 hr, and cell lysates were obtained using RIPA buffer containing 25 μL/mL protease inhibitor (Sigma-Aldrich). Proteins (20–40 μg loaded per lane) were separated by SDS-PAGE and transferred to nitrocellulose. Antibodies used were mouse anti-acetylated tubulin (1:5,000 dilution; Sigma-Aldrich), rabbit anti-β-actin (1:2,000 dilution; Abcam), rabbit anti-GSK-3β (1:1,000 dilution; Cell Signaling Technology), rabbit anti-phospho GSK-3β (Ser 9) (1:100 dilution; Cell Signaling Technology), rabbit anti-GSK3 (∝+β) (phospho Y216+Y279; 1:1,000 dilution; Abcam), and secondary horseradish peroxidase (HRP)-conjugated antibodies per the manufacturer's instructions (Dako and Thermo Fisher Scientific). Proteins were detected by the addition of SuperSignal West Pico Chemiluminescent substrate (Thermo Fisher Scientific) and were visualized using the ChemiDoc MP imaging system (Bio-Rad) and Image Lab (Bio-Rad) software. Protein band intensity was analyzed using ImageJ software. The intensity of each band was normalized to the corresponding β-actin control.

### In Vivo Experiments

In vivo experiments were conducted at the Mayo Clinic Department of Immunology and ethics approval was granted by the Mayo Foundation Institutional Animal Care and Use Committee. NOD SCID mice aged 4–5 weeks were purchased from The Jackson Laboratory.

DIPG neurospheres were disaggregated with TrypLE express stable trypsin replacement enzyme without phenol red (Thermo Fisher Scientific), counted the evening before surgery, and left in culture overnight. Cells were collected immediately prior to surgery and resuspended in either 2 μL PBS (control) or 2 μL PBS containing HSV1716 at 10 PFU/cell. To establish intracranial tumors, $5 \times 10^5$ disaggregated HSJD-DIPG-007 cells (pre-treated with PBS or HSV) were stereotactically injected into the brains of two groups of 4- to 5-week-old NOD SCID mice (The Jackson Laboratory) (n = 6 per group). The injection location was −1X, −0.8Y, 5Z from the bregma.[39] Use of these coordinates targets the fourth ventricle but allows the cells to still grow and invade into the brainstem and cerebellum. Tumors were allowed to establish and mice were euthanized when they showed clinical signs of disease (i.e., severe ataxia or > 15% weight loss). After mice were euthanized, their brains were immediately harvested into 4% PFA.

### Analysis of Brain Tissue

Brains were transferred from 4% PFA to 70% ethanol and then sliced into coronal sections. Brains were embedded in paraffin, followed by sectioning to 4-μm thickness using a manual rotary microtome (Leica) and mounted on glass slides. Tissue sections were stained with H&E. Slides were analyzed with the help of a consultant neuropathologist (Dr. Azam Ismail, Department of Histopathology, St. James's University Hospital), to identify the presence of brain tumors and the invasion and migration of tumor cells into the surrounding normal brain. Images were taken using the SPOT Insight cameraand SPOT software (both from SPOT Imaging, Diagnostic Instruments) with the Leitz DMRB (Leica) microscope at ×5, ×10, or ×20 magnification.

### Statistical Analysis

Statistical analysis was carried out using Graph Pad Prism 6 software (GraphPad Software). Statistical significance between multiple groups was determined by ANOVA. Statistical significance between two groups was determined by the Student's two-tailed t test. p values < 0.05 were considered statistically significant.

## SUPPLEMENTAL INFORMATION

Supplemental Information includes four movies and can be found with this article online at http://dx.doi.org/10.1016/j.omto.2017.04.002.

## AUTHOR CONTRIBUTIONS

J.V.C. contributed to conception of the work, data collection and analysis, and writing of the article. A.B.-R., E.I., A.M., S.S., E.M., S.P., P.S., and R.V. contributed to conception of the work, data analysis, supervision, and revision of the manuscript. K.J.S., A.R., J.T., and T.K. contributed to data collection. A.I. contributed to data analysis. A.M.C. contributed to experimental design. J.C. provided the virus.

## CONFLICTS OF INTEREST

J.C. is an employee of Virttu Biologics.

## ACKNOWLEDGMENTS

We thank our primary funders Yorkshire Cancer Research, along with Children with Cancer, the PPR Foundation, and the Candlelighters Children Cancer Charity, who have also helped support this work.

## REFERENCES

1. Jones, C., Perryman, L., and Hargrave, D. (2012). Paediatric and adult malignant glioma: close relatives or distant cousins? Nat. Rev. Clin. Oncol. *9*, 400–413.
2. Louis, D.N., Ohgaki, H., Wiestler, O.D., Cavenee, W.K., Burger, P.C., Jouvet, A., Scheithauer, B.W., and Kleihues, P. (2007). The 2007 WHO classification of tumours of the central nervous system. Acta Neuropathol. *114*, 97–109.
3. Fangusaro, J. (2012). Pediatric high grade glioma: a review and update on tumor clinical characteristics and biology. Front. Oncol. *2*, 105.
4. Schroeder, K.M., Hoeman, C.M., and Becher, O.J. (2014). Children are not just little adults: recent advances in understanding of diffuse intrinsic pontine glioma biology. Pediatr. Res. *75*, 205–209.
5. Hargrave, D., Bartels, U., and Bouffet, E. (2006). Diffuse brainstem glioma in children: critical review of clinical trials. Lancet Oncol. *7*, 241–248.
6. Khatua, S., Moore, K.R., Vats, T.S., and Kestle, J.R. (2011). Diffuse intrinsic pontine glioma-current status and future strategies. Childs Nerv. Syst. *27*, 1391–1397.
7. Cockle, J.V., Picton, S., Levesley, J., Ilett, E., Carcaboso, A.M., Short, S., Steel, L.P., Melcher, A., Lawler, S.E., and Brüning-Richardson, A. (2015). Cell migration in paediatric glioma; characterisation and potential therapeutic targeting. Br. J. Cancer *112*, 693–703.
8. Louis, D.N. (2006). Molecular pathology of malignant gliomas. Annu. Rev. Pathol. *1*, 97–117.
9. Demuth, T., and Berens, M.E. (2004). Molecular mechanisms of glioma cell migration and invasion. J. Neurooncol. *70*, 217–228.
10. Russell, S.J., Peng, K.W., and Bell, J.C. (2012). Oncolytic virotherapy. Nat. Biotechnol. *30*, 658–670.
11. Prestwich, R.J., Harrington, K.J., Pandha, H.S., Vile, R.G., Melcher, A.A., and Errington, F. (2008). Oncolytic viruses: a novel form of immunotherapy. Expert Rev. Anticancer Ther. *8*, 1581–1588.
12. Radtke, K., Döhner, K., and Sodeik, B. (2006). Viral interactions with the cytoskeleton: a hitchhiker's guide to the cell. Cell. Microbiol. *8*, 387–400.
13. Taylor, M.P., Koyuncu, O.O., and Enquist, L.W. (2011). Subversion of the actin cytoskeleton during viral infection. Nat. Rev. Microbiol. *9*, 427–439.
14. Naghavi, M.H., Gundersen, G.G., and Walsh, D. (2013). Plus-end tracking proteins, CLASPs, and a viral Akt mimic regulate herpesvirus-induced stable microtubule formation and virus spread. Proc. Natl. Acad. Sci. USA *110*, 18268–18273.
15. Lyman, M.G., and Enquist, L.W. (2009). Herpesvirus interactions with the host cytoskeleton. J. Virol. *83*, 2058–2066.
16. Wollmann, G., Ozduman, K., and van den Pol, A.N. (2012). Oncolytic virus therapy for glioblastoma multiforme: concepts and candidates. Cancer J. *18*, 69–81.
17. Rampling, R., Cruickshank, G., Papanastassiou, V., Nicoll, J., Hadley, D., Brennan, D., Petty, R., MacLean, A., Harland, J., McKie, E., et al. (2000). Toxicity evaluation of replication-competent herpes simplex virus (ICP 34.5 null mutant 1716) in patients with recurrent malignant glioma. Gene Ther. *7*, 859–866.
18. Papanastassiou, V., Rampling, R., Fraser, M., Petty, R., Hadley, D., Nicoll, J., Harland, J., Mabbs, R., and Brown, M. (2002). The potential for efficacy of the modified (ICP 34.5(-)) herpes simplex virus HSV1716 following intratumoural injection into human malignant glioma: a proof of principle study. Gene Ther. *9*, 398–406.
19. Harrow, S., Papanastassiou, V., Harland, J., Mabbs, R., Petty, R., Fraser, M., Hadley, D., Patterson, J., Brown, S.M., and Rampling, R. (2004). HSV1716 injection into the brain adjacent to tumour following surgical resection of high-grade glioma: safety data and long-term survival. Gene Ther. *11*, 1648–1658.
20. Kaufman, H.L., Kohlhapp, F.J., and Zloza, A. (2015). Oncolytic viruses: a new class of immunotherapy drugs. Nat. Rev. Drug Discov. *14*, 642–662.
21. Etienne-Manneville, S. (2013). Microtubules in cell migration. Annu. Rev. Cell Dev. Biol. *29*, 471–499.
22. Etienne-Manneville, S. (2010). From signaling pathways to microtubule dynamics: the key players. Curr. Opin. Cell Biol. *22*, 104–111.
23. Kirschner, M., and Mitchison, T. (1986). Beyond self-assembly: from microtubules to morphogenesis. Cell *45*, 329–342.
24. Bartolini, F., and Gundersen, G.G. (2010). Formins and microtubules. Biochim. Biophys. Acta *1803*, 164–173.
25. Schulze, E., and Kirschner, M. (1987). Dynamic and stable populations of microtubules in cells. J. Cell Biol. *104*, 277–288.
26. Peris, L., Wagenbach, M., Lafanechère, L., Brocard, J., Moore, A.T., Kozielski, F., Job, D., Wordeman, L., and Andrieux, A. (2009). Motor-dependent microtubule disassembly driven by tubulin tyrosination. J. Cell Biol. *185*, 1159–1166.
27. Reed, N.A., Cai, D., Blasius, T.L., Jih, G.T., Meyhofer, E., Gaertig, J., and Verhey, K.J. (2006). Microtubule acetylation promotes kinesin-1 binding and transport. Curr. Biol. *16*, 2166–2172.
28. Tran, A.D., Marmo, T.P., Salam, A.A., Che, S., Finkelstein, E., Kabarriti, R., Xenias, H.S., Mazitschek, R., Hubbert, C., Kawaguchi, Y., et al. (2007). HDAC6 deacetylation of tubulin modulates dynamics of cellular adhesions. J. Cell Sci. *120*, 1469–1479.
29. Liao, G., Nagasaki, T., and Gundersen, G.G. (1995). Low concentrations of nocodazole interfere with fibroblast locomotion without significantly affecting microtubule level: implications for the role of dynamic microtubules in cell locomotion. J. Cell Sci. *108*, 3473–3483.
30. Waterman-Storer, C.M., Salmon, W.C., and Salmon, E.D. (2000). Feedback interactions between cell-cell adherens junctions and cytoskeletal dynamics in newt lung epithelial cells. Mol. Biol. Cell *11*, 2471–2483.
31. Ganguly, A., Yang, H., Sharma, R., Patel, K.D., and Cabral, F. (2012). The role of microtubules and their dynamics in cell migration. J. Biol. Chem. *287*, 43359–43369.
32. Dumontet, C., and Jordan, M.A. (2010). Microtubule-binding agents: a dynamic field of cancer therapeutics. Nat. Rev. Drug Discov. *9*, 790–803.
33. Sun, T., Rodriguez, M., and Kim, L. (2009). Glycogen synthase kinase 3 in the world of cell migration. Dev. Growth Differ. *51*, 735–742.
34. Grimes, C.A., and Jope, R.S. (2001). The multifaceted roles of glycogen synthase kinase 3beta in cellular signaling. Prog. Neurobiol. *65*, 391–426.
35. Luo, J. (2009). Glycogen synthase kinase 3beta (GSK3beta) in tumorigenesis and cancer chemotherapy. Cancer Lett. *273*, 194–200.
36. Etienne-Manneville, S., and Hall, A. (2003). Cdc42 regulates GSK-3beta and adenomatous polyposis coli to control cell polarity. Nature *421*, 753–756.
37. Cockle, J.V., Picton, S.V., and Melcher, A. (2013). Future clinical potential of oncolytic virotherapy for pediatric CNS tumors. CNS Oncol. *2*, 307–310.
38. Turnbull, S., West, E.J., Scott, K.J., Appleton, E., Melcher, A., and Ralph, C. (2015). Evidence for oncolytic virotherapy: where have we got to and where are we going? Viruses *7*, 6291–6312.
39. Caretti, V., Zondervan, I., Meijer, D.H., Idema, S., Vos, W., Hamans, B., Bugiani, M., Hulleman, E., Wesseling, P., Vandertop, W.P., et al. (2011). Monitoring of tumor growth and post-irradiation recurrence in a diffuse intrinsic pontine glioma mouse model. Brain Pathol. *21*, 441–451.